

Microstructure of frontoparietal connections predicts individual resistance to sleep deprivation



Jiaolong Cui^{a,b}, Olga Tkachenko^a, Hannah Gogel^a, Maia Kipman^a, Lily A. Preer^a, Mareen Weber^{a,b}, Shreya C. Divatia^a, Lauren A. Demers^a, Elizabeth A. Olson^{a,b}, Jennifer L. Buchholz^a, John S. Bark^a, Isabelle M. Rosso^{a,b}, Scott L. Rauch^{a,b}, William D.S. Killgore^{a,b,c,*}

^a Social, Cognitive and Affective Neuroscience Lab, McLean Hospital, Belmont, MA, USA

^b Department of Psychiatry, Harvard Medical School, Boston, MA, USA

^c Department of Psychiatry, University of Arizona, Tucson, AZ, USA

ARTICLE INFO

Article history:

Accepted 14 November 2014

Available online 21 November 2014

Keywords:

Sleep deprivation

Diffusion tensor imaging

Functional MRI

Working memory

Fiber tractography

Superior longitudinal fasciculus

Fronto-parietal activation

ABSTRACT

Sleep deprivation (SD) can degrade cognitive functioning, but growing evidence suggests that there are large individual differences in the vulnerability to this effect. Some evidence suggests that baseline differences in the responsiveness of a fronto-parietal attention system that is activated during working memory (WM) tasks may be associated with the ability to sustain vigilance during sleep deprivation. However, the neurocircuitry underlying this network remains virtually unexplored. In this study, we employed diffusion tensor imaging (DTI) to investigate the association between the microstructure of the axonal pathway connecting the frontal and parietal regions—i.e., the superior longitudinal fasciculus (SLF)—and individual resistance to SD. Thirty healthy participants (15 males) aged 20–43 years underwent functional magnetic resonance imaging (fMRI) and diffusion tensor imaging (DTI) at rested wakefulness prior to a 28-hour period of SD. Task-related fronto-parietal fMRI activation clusters during a Sternberg WM Task were localized and used as seed regions for probabilistic fiber tractography. DTI metrics, including fractional anisotropy, mean diffusivity, axial and radial diffusivity were measured in the SLF. The psychomotor vigilance test (PVT) was used to evaluate resistance to SD. We found that activation in the left inferior parietal lobule (IPL) and dorsolateral prefrontal cortex (DLPFC) positively correlated with resistance. Higher fractional anisotropy of the left SLF comprising the primary axons connecting IPL and DLPFC was also associated with better resistance. These findings suggest that individual differences in resistance to SD are associated with the functional responsiveness of a fronto-parietal attention system and the microstructural properties of the axonal interconnections.

© 2014 Published by Elsevier Inc.

Introduction

Sleep deprivation (SD), even for one night, can lead to impairments in cognitive function and performance (Killgore, 2010). It has been found that individual differences in resistance to cognitive performance impairment following SD are consistent, trait-like, and stable over time (Rupp et al., 2012; Van Dongen et al., 2004). Numerous neuroimaging studies suggest that task-related activation in frontal and parietal cortices is particularly susceptible to the effects of SD and related to alterations in cognitive performance during SD (Chee and Choo, 2004; Choo et al., 2005). Moreover, several studies have reported that the extent of fronto-parietal activation in response to a working memory (WM) task under normal well-rested conditions can predict the magnitude of activation change and performance decline after SD (Caldwell

et al., 2005; Chee et al., 2006; Lythe et al., 2012; Mu et al., 2005). However, the structure–function relationship underlying this fronto-parietal network in SD is not well understood. Most studies regarding the effects of SD on cognitive functioning have focused primarily on changes in functional brain activation, but much less is known about the microstructural properties of white matter fiber tracts underlying the fronto-parietal brain regions typically affected by sleep loss. Of particular interest is the association between individual resistance to SD and the microstructure of the superior longitudinal fasciculus (SLF), a primary and direct tract supporting bidirectional information transfer between the frontal and parietal cortices (Schmahmann and Pandya, 2006).

Diffusion tensor imaging (DTI) enables an in vivo characterization of microstructural properties of white matter based on water molecular diffusion (Basser et al., 1994; Hagmann et al., 2006). Water tends to diffuse preferentially in a direction parallel to the orientation of axons (Basser, 1995; Beaulieu, 2002). This phenomenon is called diffusion anisotropy and is represented by a diffusion tensor model. The tensor has

* Corresponding author at: Social, Cognitive, and Affective Neuroscience Lab, Department of Psychiatry, University of Arizona, Tucson, AZ 85724, USA.

E-mail address: Killgore@psychiatry.arizona.edu (W.D.S. Killgore).

three eigenvalues that represent the magnitude of diffusion in three axis directions (Hagmann et al., 2006). The most commonly used parameter in DTI analysis, fractional anisotropy (FA), is calculated from the three eigenvalues to indicate the degree of anisotropy of the diffusion tensor. FA is a scalar value that ranges from 0 (low) to 1 (high) and reflects axon caliber, degree of myelination, and axon density within a voxel (Beaulieu, 2002). Higher FA values represent better microarchitecture of the white matter tracts. The average of the three eigenvalues is called mean diffusivity and is considered an estimation of membrane density (Schmithorst and Yuan, 2010). The largest eigenvalue, indicating diffusion along the direction of the axons, is termed axial diffusivity (AD), which may reflect aspects of axon morphology and pathology including axon diameter, loss, or damage (Budde et al., 2007; Song et al., 2003). The average of the other two eigenvalues provides a measure of radial diffusivity (RD), which is considered to reflect the degree of myelination (Nair et al., 2005; Song et al., 2002).

To our knowledge, only one study has used DTI to investigate the relationship between white matter integrity and cognitive vulnerability to SD (Rocklage et al., 2009). Higher FA values were found in SD-resilient compared to SD-vulnerable groups in multiple white matter regions, including the corpus callosum, forceps major, posterior limb of the internal capsule, retrolenticular portion of the internal capsule, superior corona radiata, posterior corona radiata, SLF, posterior thalamic radiation, and corticospinal tract (CST), but these were not linked to functional responses in that study. No DTI studies have yet explored the specific relationship between resistance to SD and microstructural architecture of white matter fiber tracts, and none have linked structural indices with known functional regions, such as those involved in sustained attention or working memory, to identify potential structure–function networks that may predict cognitive resistance to sleep loss. In this study, we aimed to determine if the microstructural properties of the SLF, which connects primary attention and vigilance regions, might be associated with SD resistance. At rested baseline, we measured the DTI metrics of this tract of interest (TOI) using the Johns Hopkins University (JHU) white matter atlas and also employed probabilistic fiber tractography to reconstruct the specific white matter tracts connecting fronto-parietal activated regions identified with WM task-related functional MRI (fMRI). Participants were then sleep deprived for one night and their cognitive vigilance was monitored hourly throughout the night using the gold standard psychomotor vigilance test (PVT) to determine individual resistance to SD (Dinges and Powell, 1985). For each participant, a simple resistance score was calculated by determining the mean percent decline in PVT performance speed during the overnight sleep deprivation period compared to baseline. After identifying functionally defined frontal–parietal attention regions, we correlated the DTI metrics of the SLF with individual resistance scores. We hypothesized that individuals with higher FA values of the SLF tracts connecting functionally activated fronto-parietal attention regions would demonstrate greater resistance to SD.

Methods

Participants

Thirty-four right-handed, healthy, native English-speaking adults (mean age 25.4 ± 5.8 years, range 20–43; 17 males, 16 females) were recruited from the greater Boston area and underwent neuroimaging. Exclusion criteria included any history of self-reported medical, neurological, psychiatric, or sleep disorders. Data from four participants were excluded due to poor image quality. The final analyzed group consisted of 30 subjects (mean age 25.8 ± 6.0 years, range 20–43; 15 males, 15 females). All participants provided written informed consent prior to participation and were compensated for their time. This research protocol was reviewed and approved by the Institutional Review Board of McLean Hospital and the U.S. Army Human Research Protection Office.

Materials and procedure

Participants were scheduled for three visits. The procedure for this experiment can be seen in Fig. 1A. The first visit was a baseline session during which volunteers were informed of the study procedures and underwent screening for the presence of psychopathology using the Mini International Neuropsychiatric Interview (MINI) (Sheehan et al., 1998).

After seven to ten days ($M = 8.44$, $SD = 3.19$), participants returned to the lab for the imaging session. Caffeine use was determined via a questionnaire that asked participants to list their frequency of use of caffeine related products per day, including from coffee (8 oz), brewed tea (8 oz), caffeinated soda (cans), caffeinated sports drinks (per bottle/can), and over the counter caffeine supplements. We scored these according to the values provided in Killgore (2011). Based on these criteria, participants were found to be low to moderate users of caffeine, with an average intake of 62.1 mg per day ($SD = 83.8$; range = 0–266 mg). Of the sample, 13 participants (43.3%) reported no regular consumption of caffeine containing products, with 8 participants (26.7%) reporting greater than 100 mg of caffeine per day. On the day of the scan, participants were not asked to refrain from caffeine consumption. Instead, they were asked to consume their “normal” morning caffeine, so that they would not be in any form of withdrawal during the scan. On the day of the scan, participants consumed an average of 46.7 mg ($SD = 78.7$ mg) prior to arrival to the neuroimaging session. In order to control for fluctuations due to menstrual hormones, all female participants were either on monophasic contraceptives or were scheduled to undergo neuroimaging during the follicular phase of the menstrual cycle. In addition, participants were asked not to take any over-the-counter medication on the day of this session.

The third lab visit, a 28-hour sleep deprivation session, began on the Friday following the second visit. The time between the scan and the overnight sleep deprivation session ranged from one to four days ($M = 2.23$, $SD = 1.45$). On the two nights before the final sleep deprivation session, participants were instructed to go to bed between 10 and 11 pm and remain in bed for 8 h each night and were asked to abstain from any caffeine-containing products or other stimulants. On the morning of the third visit day, participants were required to rise between 7:00 am and 8:00 am (verified by actigraphy sleep data and sleep diaries). Every participant was given a wake-up call at 7:30 am and was required to remain awake for the next 28 to 30 h until being released from the study at 12:00 pm the following day. Participants arrived at the McLean Hospital Sleep Research Laboratory by 6:30 pm and completed the overnight SD sessions in pairs (1 male and 1 female). Beginning at 7:15 pm, a modified 10-minute version of the psychomotor vigilance test (PVT) was administered on a laptop computer every hour throughout the SD session (Dinges and Powell, 1985). The testing sessions were run simultaneously for both participants in separate rooms. During the PVT, participants monitored a screen and pressed a response button as quickly as possible each time a target stimulus appeared. Response time feedback was given after each response. The interstimulus interval was varied pseudorandomly between presentations to minimize anticipation of the stimulus (ITI range: 2 to 10 s). Reaction time (RT) and number of attentional lapses ($RT \geq 500$ ms) for all trials were collected.

Sternberg working memory task (SWMT)

The SWMT was performed during the fMRI scan and the behavioral data were acquired within the scanner. Each functional scan lasted for 12 min and 58 s, consisting of an initial 10-second fixation cross followed by twelve (12) 64-second stimulus blocks. Each block included a 32-second control task followed by a 32-second Sternberg task. Each task comprised two 16-second trials. During the task, participants were asked to press an MR compatible button box to respond YES or NO to each trial following a visual prompt. The RT was defined as the time

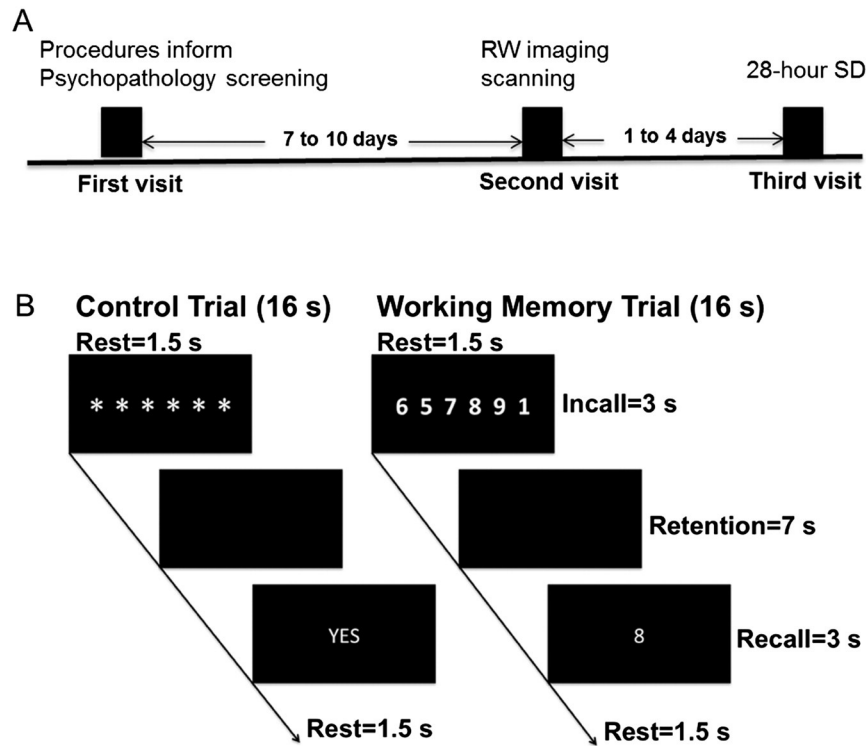


Fig. 1. A: Schematic showing the order of the complete experimental protocol. Briefly, participants underwent three sessions including the first visit: experiment procedures inform and psychopathology screening; second visit: neuroimaging scanning at rested wakefulness; third visit: 28 h of sleep deprivation. RW, rested wakefulness; SD, sleep deprivation. B: Example of subcomponents of a control trial and a Sternberg working memory trial. Each 16-second trial includes 3-second encoding, 7-second retention, 3-second recall and 1.5-second rest period in the onset and end of each trial.

from onset of the presentation to the participant's response. During the WM trials, a row of 1, 3, or 6 digits was randomized to display on the screen. Participants viewed the set of digits for 3 s (encoding), and maintained them in mind for a 7 second delay period (retention), during which the screen was blank. Subsequently, a digit was presented on the screen for 3 s, and participants responded *YES* or *NO* according to whether this digit had been included in the previously viewed digit set (recall). There was a 1.5-second rest period at the beginning and end of each trial. The control trials consisted of a 3-second viewing of 6 asterisks, followed by a 7-second delay, and then a 3-second screen presentation of the word *YES* or *NO* presented in the center of the screen (Fig. 1B). Participants were asked to press the button corresponding to the word displayed on the screen.

Magnetic resonance imaging parameters

Scans were collected using a 3.0 Tesla Siemens Tim Trio scanner (Siemens, Erlangen, Germany) and a 32-channel head coil. Structural T1-weighted 3D magnetization-prepared rapid gradient-echo (MPRAGE) images were collected over 176 sagittal slices (TR/TE/flip angle = 2.1 s/2.25 ms/12°, 256 × 256 matrix) with voxel size = 1 × 1 × 1 mm. T2*-weighed functional MRI scans were collected over 34 transverse slices (3.5 mm thickness, no gap) using an interleaved sequence, TR/TE/flip angle = 2.0 s/30 ms/90°, with 60 images collected per slice. Data were collected with a 22.4 cm field of view (FOV), a 64 × 64 acquisition matrix, and a voxel size of 3.5 × 3.5 × 3.5 mm. Whole brain DTI was acquired using a single-shot echo-planar imaging sequence. Forty transverse slices were acquired with the following parameters: FOV = 80 mm, acquisition matrix = 128 × 128, TR/TE = 6340 s/99 ms, voxel size = 1.75 × 1.75 × 3.5 mm, and number of acquisitions = 1. Eight b = 0 images were acquired and diffusion

gradients were applied in 72 directions uniformly distributed on a sphere with b = 1000 s/mm².

Functional image processing

Blood oxygenation level-dependent (BOLD) data were preprocessed and analyzed in SPM8 (Wellcome Department of Cognitive Neurology, London, UK; <http://www.fil.ion.ucl.ac.uk/spm>). Raw images were realigned to the first image in the series, unwarped, registered to each participant's high-resolution anatomical image, and normalized to the 3D space of the Montreal Neurological Institute (MNI). Data were spatially smoothed with an isotropic Gaussian kernel (full width half maximum (FWHM) = 6 mm) and resliced to 2 × 2 × 2 mm³ voxel size using 4th Degree B-Spline interpolations. The time series data were convolved with the SPM8 canonical hemodynamic response function, the AR(1) option was used to correct for serial autocorrelation, and a 128-second high-pass filter was used to remove low-frequency confounds. The Artifact Detection Tool (http://www.nitrc.org/projects/artifact_detect/) implemented in the SPM8 toolbox was employed for comprehensive analysis of artifacts in time series data including spiking and motion. Scan volumes exceeding 3 SD in mean global intensity, or scan-to-scan motion that exceeded 1.0 mm, and the first volume of each run were regressed out of the first-level analysis as nuisance covariates. Within SPM, a series of general linear models was created for the 1-digit, 3-digit, 6-digit, and control conditions. Contrast images of n-digit (n = 1, 3, 6) versus control were then created. These contrast images were then taken into a second-level random effects analysis via one-sample t-tests to identify regions of greater responsiveness of the brain to n-digit working memory than the control condition. We identified clusters of activation as areas containing at least 100 contiguous voxels, thresholded at a whole-brain voxelwise false discovery rate (FDR) correction of p < 0.01. Parameter estimates (mean beta value)

were extracted for each activation cluster via the region extraction (REX) tool (<https://www.nitrc.org/projects/rex/>). Each activation cluster was defined as a functional region of interest (ROI). The ROIs defined from the SWMT fMRI were used as seed regions in the diffusion tensor fiber tractography.

Diffusion image processing

DTI data were processed with the FSL 5.0.4 Diffusion Toolbox (FDT, <http://www.fmrib.ox.ac.uk/fsl/fdt/>) (Smith et al., 2004). A standard FDT multistep procedure was adopted including: 1) image quality check: any gradient directions with signal dropouts caused by excessive motion were removed and not included in the analysis; 2) motion and eddy current correction; 3) correction of gradient directions for any image rotation during the previous motion and eddy current correction; 4) removal of skull and nonbrain tissue using the Brain Extraction Tool (BET, <http://fsl.fmrib.ox.ac.uk/fsl/fslwiki/BET>) (Smith, 2002); 5) tensor reconstruction using weighted least squares fit was performed via DTIFit within FDT to create DTI scalar images, including the FA, MD and three eigenvalues. The RD maps were computed as the average of the two minor eigenvalue images; and 6) nonlinear alignment of each participant's volume to the standard Montreal Neurological Institute (MNI152) space template by FNIRT. Mean FA, MD, AD, and RD values were extracted from bilateral SLF using the JHU White Matter atlas (JHU-ICBM-tracts-maxprob-thr50-1 mm, provided by FSL) (Hua et al., 2008). In order to examine whether other non-hypothesized primary tracts might be associated with cognitive resistance to SD, additional analyses also measured the DTI metrics in forceps major, forceps minor, bilateral cingulum, anterior thalamic radiation (ATR), CST, inferior longitudinal fasciculus (ILF), inferior fronto-occipital fasciculus (IFOF) and uncinate fasciculus (UNC). These were conducted as exploratory analyses.

Fiber tracking was performed using a probabilistic tractography algorithm implemented in FSL (ProbtrackX) (Behrens et al., 2007). First, diffusion parameters were estimated at each voxel using BedpostX. ProbtrackX was then used to estimate the distribution of connections between seed and target regions. To generate this connectivity distribution, 5000 streamline samples were initiated, traveling along the probability distribution functions of local voxels with a step length of 0.5 mm and a curvature threshold of 0.2. We used localized regions activated during the SWMT fMRI as seed regions (Kim and Kim, 2005). Seed regions were transformed from standard space (MNI152 2-mm³ standard brain) to each individual diffusion space using a nonlinear transform (standard2diff) with 12 degrees of freedom. Since we were interested in the direct pathways between frontal and parietal regions, a pair of anterior and posterior regions in the same hemisphere was used as paired seeds. Generated pathways are volumes in which values at each voxel represent the number of streamlines passing through that voxel and, therefore, the probability of connection between paired seed regions. To remove background noise, pathways in each individual were thresholded to include only voxels with at least 100 samples passing through them (out of 5000 initiated streamline samples) (Johansen-Berg et al., 2007). Pathways in each subject were then binarized and overlaid to produce population probability maps for each pathway, in which voxel values represent the number of participants in whom a pathway is present. The population probability maps were thresholded at 50% of the maximum number of participants (MNP) who had overlapping connections between paired seed regions to generate a group tract map (Mayer and Vuong, 2013). The obtained group tract map was then transformed to individual diffusion space and binarized to mask the FA, MD, AD, and RD maps for DTI metrics measurement.

Statistical analysis

Two metrics were used to evaluate resistance to SD (Loh et al., 2004), including PVT Speed ((1/RT)*1000), and attentional lapses. For

the purpose of this analysis, the first 5 PVT sessions (7 pm–11 pm) were used as the baseline, given that 11 pm is often the point at which vigilance changes begin to emerge following a normal day of wakefulness (Wesensten et al., 2005). The mean PVT speed demonstrated during the subsequent 12 h (from 12 am to 11 am) was assessed as sleep-deprived performance (see Supplementary Fig. 1) (Loh et al., 2004). Percentage reaction speed change (PRSC) was calculated as $PRSC = (\text{reaction speed from 12 am to 11 am}) / (\text{reaction speed from 7 pm to 11 pm}) \times 100\%$. Greater mean PRSC values during SD represent greater resistance capacity. Additionally, the total number of lapses during SD was taken as a second index of resistance. Specifically, the sum of attentional lapses for each participant was square root transformed to have a normal distribution. Initially, age and gender were included as nuisance covariates, but were found to be unrelated with acquired task-related activation and DTI metrics. Therefore, these covariates were excluded from further analyses. Pearson correlation with the significance level at Bonferroni corrected $p < 0.05$ was conducted to analyze the linear association between imaging metrics and behavioral assessment using SPSS Statistics 20 (IBM Corporation, Armonk, New York, USA).

Results

Behavioral assessment

Demographic and behavioral features of our sample are summarized in Table 1. For the PVT, individual PRSC from the baseline cognitive performance ranged from 68.1% to 100% (mean \pm SD: 88.2% \pm 8.3%) and the mean frequency of attentional lapses at each session ranged from 1.0 to 18.9 (mean \pm SD: 8.6 \pm 4.7).

In the SWMT, longer RT was found in trials with greater memory load (see Table 1). One-way ANOVA revealed a significant effect of memory load ($F = 14.94$, $p < 0.001$). In addition, it was found that PRSC was significantly negatively correlated with RT in the control ($r = -.526$; $p = .003$) and 1-digit tasks ($r = -.466$; $p = .011$). PRSC also showed a strong trend with RT in the 3-digit ($r = -.350$; $p = .063$) and 6-digit tasks ($r = -.358$; $p = .057$). Lapses showed significant positive correlation with RT in the control ($r = .535$; $p = .003$) and 1-digit tasks ($r = .506$; $p = .005$) while there were no significant correlations with 3-digit ($r = .362$; $p = .053$) or 6-digit task ($r = .157$; $p = .416$). Self-reported daily caffeine intake and caffeine intake on the morning of the scan were unrelated to performance on any of the SWMT variables (all p -values $> .10$).

Fronto-parietal activation to SWMT correlates with resistance

As shown in Fig. 2, significant activation (6-digit task $>$ control task) was found in the right ventrolateral prefrontal cortex (VLPFC) (Brodmann area (BA): 13, 47), left VLPFC (BA: 13, 47), left dorsolateral

Table 1
Demographic and behavioral data from participants.

	Mean	SD	Range
<i>Demographic data</i>			
Age	25.8	6.0	20–43
Gender (male/female)	15/15		
<i>Reaction time in SWMT</i>			
Control	682.3	163.4	416.3–1057.5
1-digit	790.2	253.2	447.5–1518.8
3-digit	910.0	270.6	481.5–1735.4
6-digit	1100.0	318.5	558.8–1617.9
<i>Psychomotor vigilance test</i>			
PRSC	88.2%	8.3%	68.1%–100%
Lapses	8.6	4.7	1.0–18.9

SWMT, Sternberg working memory test. Reaction time in SWMT is in millisecond; PRSC, percentage reaction speed change.

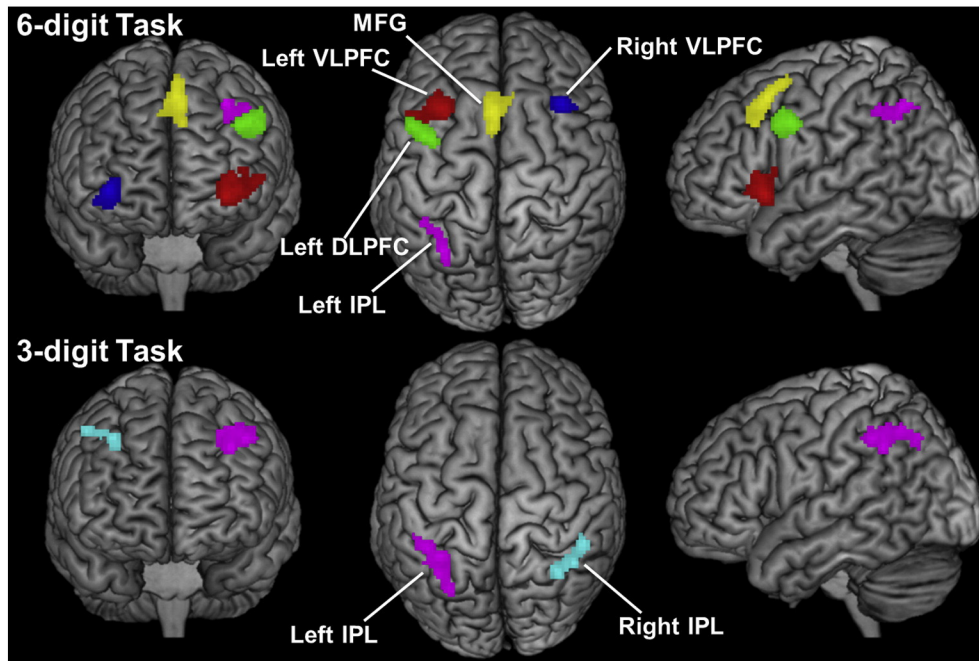


Fig. 2. Result of the fMRI analysis for SWMT. Coordinates are in MNI space. Clusters of activation were defined as areas containing at least 100 contiguous voxels, thresholded at whole brain voxelwise false discovery rate (FDR) $p < 0.01$. Significant activation (6-digit SWMT > control task) was found in left VLPFC (red), left DLPFC (green), left IPL (violet), MFG (yellow) and right VLPFC (blue) (top row). Significant activation (3-digit SWMT > Control task) was found in left IPL (violet), and right IPL (cyan) (bottom row). No significant activation was found for 1-digit SWMT > Control task. SWMT, Sternberg working memory task; MNI, Montreal Neurological Institute; VLPFC, ventrolateral prefrontal cortex; DLPFC, dorsolateral prefrontal cortex; IPL, inferior parietal lobule; MFG, medial frontal gyrus.

prefrontal cortex (DLPFC) (BA: 9), left inferior parietal lobule (IPL) (BA: 7, 40) and medial frontal gyrus (MFG) (BA: 6, 8, 32). Performing the 3-digit task compared to the control task resulted in significant activation in the left IPL (BA: 7, 40) and right IPL (BA: 40). No significant activation was found in response to the 1-digit task compared to the control task. The details of the significant activations are summarized in Table 2.

As shown in Fig. 3, the activation in the left IPL (MNI: $-32, -60, 46$) and the left DLPFC (MNI: $-42, 4, 36$) responses to the 6-digit SWMT on the day of scanning were significantly positively correlated with PRSC (left IPL: $r = .36, p = .05$; left DLPFC: $r = .41, p = .02$) and significantly negatively correlated with number of lapses on the PVT (left IPL: $r = -.37, p = .04$; left DLPFC: $r = -.45; p = .01$) during sleep deprivation. The remaining clusters of activity on the 6-digit and 3-digit SWMT tasks were not significantly correlated with PVT performance ($p > .05$).

TOI-based measures of DTI metrics in the left SLF correlate with resistance

The mean FA, MD, AD, and RD values were measured in each TOI (see Supplementary Table 1). As shown in Fig. 4, average FA in the left SLF showed a significant positive correlation with PRSC ($r = .38, p = .04$) and a strong negative trend with lapses ($r = -.34, p = .07$).

Average MD in the left SLF was significantly negatively correlated with PRSC ($r = -.51, p < .01$) and showed a trend association with lapses ($r = .31, p = .09$; see Table 3). Average RD in the left SLF was significantly negatively correlated with PRSC ($r = -.49, p < .01$) and positively correlated with lapses ($r = .38, p = .04$). Aside from the left SLF, there were no significant correlations between behavioral assessments and DTI metrics in the other tracts ($p > .05$), except for the right SLF, where average MD was negatively correlated with PRSC ($r = -.47, p = .01$).

Tractography-based measures of DTI metrics in the left SLF correlate with resistance

Activation clusters found in SWMT-related fMRI were localized as seed regions, including bilateral IPL, left DLPFC, MFG, and bilateral VLPFC. The left IPL was activated for both the 6-digit and 3-digit tasks. We chose the 6-digit task-related activation cluster as the seed region of the left IPL because it was significantly correlated with resistance. The information regarding the fiber tracts connecting the pairwise activation clusters is summarized in Table 4. The MNP value indicated the probability of connectivity between the paired seed regions. The connectivity between the left DLPFC and the left IPL showed the highest

Table 2
Regions of significant activation (N-digit vs control) in the Sternberg working memory test.

SWMT load	Brain region	BA	MNI coordinates	Cluster size	T value	Z value	Correlation with PRSC	Correlation with lapse
6-digit	Right VLPFC	13, 47	36, 22, -2	165	7.26	5.44	$r = .28; p = .13$	$r = -.28; p = .12$
	Left VLPFC	13, 47	-30, 18, -4	371	7.02	5.32	$r = .32; p = .09$	$r = -.25; p = .18$
	Left DLPFC	9	-42, 4, 36	222	5.83	4.70	$r = .36; p = .05$	$r = -.37; p = .04^*$
	Left IPL	7, 40	-32, -60, 46	132	5.52	4.53	$r = .41; p = .03^*$	$r = -.45; p = .01^*$
	MFG	6, 8, 32	-4, 16, 50	276	5.83	4.71	$r = .15; p = .42$	$r = -.25; p = .19$
3-digit	Right IPL	40	32, -56, 40	125	6.04	4.82	$r = -.06; p = .74$	$r = .14; p = .45$
	Left IPL	7, 40	-32, -48, 36	317	5.81	4.70	$r = .10; p = .59$	$r = .18; p = .36$
1-digit	NS							

The threshold for identified clusters of activation was false discovery rate corrected $p < 0.01$ and k (extent) ≥ 100 contiguous voxels. BA, Brodmann area; MNI, Montreal Neurological Institute; PRSC, percentage reaction speed change; VLPFC, ventrolateral prefrontal cortex; DLPFC, dorsolateral prefrontal cortex; IPL: inferior parietal lobule; MFG, medial frontal gyrus; NS, not significant. “*” indicates $p < 0.05$.

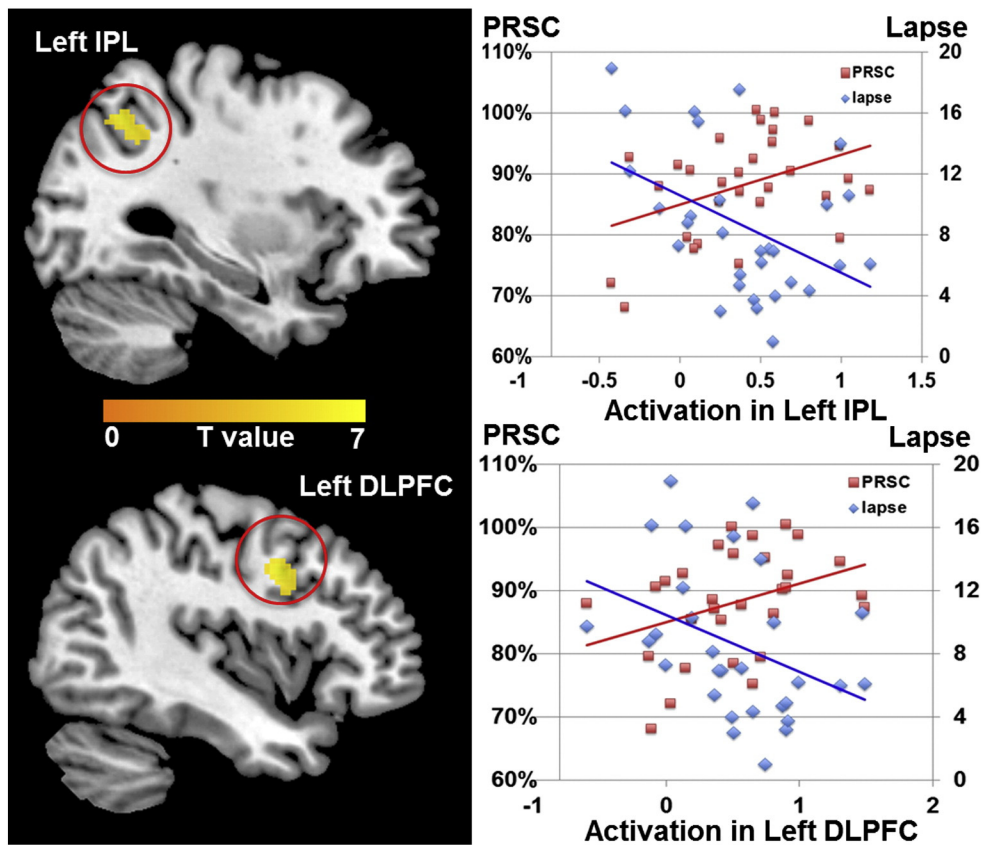


Fig. 3. Scatterplots demonstrating the relationship between the extracted cluster of activation in the left IPL versus PRSC ($r = .36$, $p = .05$) and lapses ($r = -.37$, $p = .04$) (top row) and the activation in the left DLPFC versus PRSC ($r = .41$, $p = .02$) and lapses ($r = -.45$, $p = .01$) (bottom row). PRSC, percentage reaction speed change; IPL: inferior parietal lobule; DLPFC, dorsolateral prefrontal cortex.

level of probability (MNP = 26). Bilateral VLPFC showed a higher level of connectivity to bilateral IPL (left: MNP = 19; right: MNP = 23) compared to the connectivity between MFG and bilateral IPL (left: MNP = 4; right: MNP = 5). An example of population probability maps of the reconstructed tract (or parts of the left SLF) connecting the left DLPFC and the left IPL is provided in Fig. 5. Moreover, the FA and RD values extracted from the DLPFC-IPL tract were significantly correlated with PRSC (FA: $r = .41$; $p = .02$; RD: $r = -.36$, $p = .05$). There was no significant correlation between resistance and DTI metrics extracted from the other tracts. The correlations between DTI metrics of the reconstructed tracts and the activation of seed regions were also summarized in Table 4. It was found that the DTI metrics were not associated with the activations of the seed regions ($p > 0.05$).

Discussion

The present study extends the investigation of neural correlates of resistance to SD from brain activation to metrics of microstructural architecture of the axonal fiber tracts. We used fMRI to examine the relationship of resistance to SD with functional brain activation during a working memory task. We also employed DTI and probabilistic tractography to examine the association between white matter microarchitecture and cognitive resistance to SD. We found that both functional activation of left fronto-parietal regions and DTI metrics of the primary fiber tracts connecting frontal and parietal coactivated brain regions were significantly correlated with resistance. This finding supports the hypothesis that resistance to SD is associated with the microstructure of the axons underlying the fronto-parietal attention network.

In 2005, Mu and colleagues reported that a sleep deprivation-resistant group (as measured by performance decline in the SWMT)

had more global brain activation at rested baseline than did the sleep deprivation-vulnerable group (Caldwell et al., 2005; Mu et al., 2005). Their finding suggested the viability of using neuroimaging to predict resilience against the cognitive degrading effects of SD. Chee and colleagues found that the activation of the left parietal and left frontal regions at rested wakefulness was protective against WM performance accuracy decline from normal sleep to SD (Chee et al., 2006). Recently, Lythe and colleagues employed an *n*-back WM task and found that frontal and parietal activity after normal sleep was correlated with the activity change following SD (Lythe et al., 2012). In line with several previous studies, we also found that greater activation in left fronto-parietal regions on a difficult working memory task at rested wakefulness was associated with resistance to SD, suggesting that the fronto-parietal network is implicated in the sustainment of cognitive ability in the context of SD. Of note, these previous studies used performance on various WM tasks to estimate the cognitive decline following SD, which may have been influenced by a learning effect from repeated administrations and intrinsic difference in aptitude (Van Dongen, 2005). In the current study, we employed the “gold standard” PVT, which provides a highly reliable and sensitive metric of the effects of SD on cognition and which exhibits neither a practice effect nor aptitude differences (Killgore, 2010; Van Dongen, 2005).

Working memory capacity is often considered to be one of the most crucial and fundamental cognitive processes upon which nearly all other cognitive capacities rely, and it is often considered to be a cornerstone of higher order executive control abilities. Our overarching hypothesis is that individuals with greater prefrontal executive control would be more capable of resisting sleep deprivation. Thus, we focused on the SWMT because it is one of the most well established tasks for assessing this capacity within the scanner and was used previously to identify resistance to sleep deprivation (Caldwell et al., 2005). In our

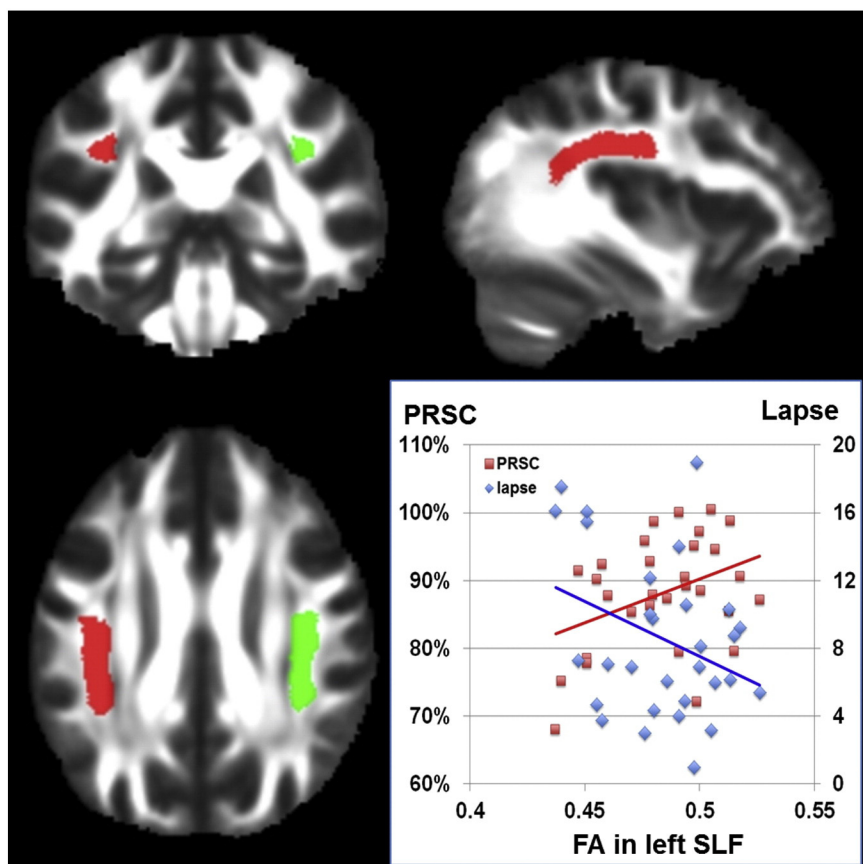


Fig. 4. Illustration of the mask of left SLF (red) and right SLF (green) provided by JHU white matter atlas in FSL, superimposed on the mean FA map of the $N = 30$ participants. Scatterplots show the relation of the FA value in the left SLF versus PRSC ($r = .38$, $p = .04$) and lapse ($r = -.34$, $p = .07$). PRSC, percentage reaction speed change; SLF, superior longitudinal fasciculus; FA, fractional anisotropy.

results, both of the activated clusters that correlated with resistance to SD (i.e., left DLPFC and left IPL) were found for the 6-digit SWMT. The activations in response to the 3-digit SWMT were not correlated with resistance to SD. The left IPL was activated in the 3-digit SWMT, but the magnitude of activation was not correlated with resistance to SD. This observation was consistent with the previous work by Lythe and colleagues, who found that the fronto-parietal activation predicting changes following SD is dependent on task load (Lythe et al., 2012). The relationship between task-related activation at rested wakefulness and WM performance is consistent with the ‘cognitive reserve hypothesis’ (Lythe et al., 2012). This suggests that individuals with greater innate cognitive capacity from the outset will have a greater reservoir of cognitive power from which to draw under conditions where cognitive resources are degraded by factors such as stress, cognitive load, age, injury, disease—or in the present case—sleep deprivation (Stern, 2002). We postulate that the high-load WM task at rested baseline can reveal the extent of individual cognitive reserve and its underlying neurocircuitry, which would then predict cognitive resistance to SD.

Our results further indicate that the microstructural properties of white matter are associated with cognitive resistance to SD, which is in accordance with the results of one previous study. Rocklage and colleagues examined white matter axonal integrity, as measured by FA, and found that it was correlated with the change in accuracy from pre-SD to post-SD during visual-motor task performance (Rocklage et al., 2009). Their analyses indicated that FA in widespread regions was predictive of cognitive vulnerability to SD. However, there was no functional investigation in their study so that they did not link these patterns to specific regions of cortical functional responsiveness. In the present study, we performed fMRI during the SWMT to explore the brain regions involved in attention and sustained vigilance

and employed probabilistic tractography to reconstruct the tracts connecting these primary brain regions, which demonstrated direct evidence that the microstructure of fronto-parietal connections was significantly correlated with resistance capacity. Specifically, we found that PRSC was positively correlated with FA and negatively correlated with RD within fiber tracts connecting left frontal and parietal regions. To examine the possibility that other white matter pathways are relevant to resistance, the DTI metrics of several white matter tracts were also measured, including the forceps major, forceps minor, bilateral cingulum, ATR, CST, ILF, IFOF and UNC, in which DTI metrics were not significantly correlated with resistance (Table 3).

By combining fMRI task activation maps and probabilistic tract reconstruction, we provide direct evidence of the involvement of a left fronto-parietal network connected by the SLF that is relevant to the capacity to sustain vigilance performance during sleep loss. Present evidence indicates that the SLF can be partitioned into subcomponents (Makris et al., 2005; Schmahmann et al., 2007): SLF-I connects medial posterior parietal cortex and the caudal superior parietal lobule (BA 7) to the supplementary motor area (SMA) and premotor area (PMA) (medial and dorsal part of the superior frontal gyrus; BA 6, 8, 9); SLF-II connects the IPL (BA 39) and intraparietal sulcus (BA 7) to dorsal PMA (BA 6), SMA (BA 8) and DLPFC (BA 9, 46); and SLF-III connects the rostral part of the IPL (BA 39) and parietal operculum (BA 40) to the ventral PMC (BA 6) and VLPFC (BA44). Because the fiber tracts were reconstructed based on the localized activated brain regions in WM task, we did not have a hypothesis regarding which subcomponent of the SLF would be most critical. Comparison between the coordinates of the reconstructed SLF in the current investigation to the results of Makris et al. suggested that the left SLF that we reconstructed is consistent with pathways comprising SLF-II and SLF-III (Makris et al., 2005).

Table 3
Correlation between DTI metrics of TOIs and behavioral assessments.

	FA		MD		AD		RD	
Hypothesized tracts								
	PRSC	Lapse	PRSC	Lapse	PRSC	Lapse	PRSC	Lapse
Left SLF	r = .38 p = .04*	r = -.34 p = .07	r = -.51 p < .01**	r = .31 p = .09	r = -.18 p = .35	r = .01 p = .97	r = -.49 p < .01*	r = .38 p = .04*
Right SLF	r = .21 p = .27	r = -.22 p = .24	r = -.47 p = .01*	r = .31 p = .09	r = -.28 p = .14	r = .10 p = .59	r = -.35 p = .06	r = .28 p = .13
Non-hypothesized tracts								
Forceps major	r = .17 p = .36	r = -.23 p = .23	r = -.22 p = .25	r = .17 p = .36	r = -.15 p = .44	r = .08 p = .67	r = -.26 p = .16	r = .25 p = .19
Forceps minor	r = .27 p = .15	r = -.20 p = .30	r = -.16 p = .40	r = .07 p = .73	r = .03 p = .88	r = -.11 p = .55	r = -.24 p = .19	r = .17 p = .36
Left ATR	r = -.03 p = .87	r = .06 p = .73	r = -.09 p = .62	r = .14 p = .48	r = -.04 p = .85	r = .09 p = .64	r = -.08 p = .66	r = .10 p = .60
Right ATR	r = .09 p = .64	r = -.10 p = .59	r = -.28 p = .13	r = .34 p = .07	r = .24 p = .19	r = .15 p = .43	r = -.34 p = .06	r = .35 p = .06
Left cingulum	r = .03 p = .87	r = .07 p = .72	r = -.16 p = .40	r = .11 p = .56	r = -.20 p = .28	r = .24 p = .21	r = -.02 p = .92	r = -.06 p = .73
Right cingulum	r = .06 p = .77	r = .01 p = .97	r = -.15 p = .41	r = .24 p = .19	r = -.17 p = .37	r = .33 p = .07	r = -.09 p = .65	r = .11 p = .58
Left CST	r = .31 p = .11	r = -.16 p = .41	r = -.24 p = .20	r = .25 p = .19	r = .05 p = .79	r = .09 p = .60	r = -.25 p = .21	r = .22 p = .25
Right CST	r = .31 p = .11	r = -.15 p = .44	r = -.32 p = .09	r = .29 p = .12	r = -.06 p = .75	r = .15 p = .42	r = -.23 p = .24	r = .23 p = .22
Left IFOF	r = .13 p = .49	r = .08 p = .67	r = -.22 p = .24	r = .21 p = .26	r = -.12 p = .54	r = .23 p = .23	r = -.20 p = .28	r = .07 p = .73
Right IFOF	r = .07 p = .72	r = .11 p = .55	r = -.33 p = .08	r = .04 p = .83	r = -.34 p = .07	r = .34 p = .06	r = -.21 p = .25	r = .08 p = .68
Left ILF	r = .30 p = .10	r = -.15 p = .44	r = -.27 p = .15	r = .04 p = .83	r = -.07 p = .73	r = -.03 p = .87	r = -.26 p = .17	r = .06 p = .74
Right ILF	r = -.12 p = .54	r = .24 p = .21	r = -.35 p = .06	r = .12 p = .53	r = -.35 p = .06	r = .29 p = .12	r = -.08 p = .66	r = -.12 p = .54
Left UNC	r = -.09 p = .65	r = .11 p = .56	r = .01 p = .96	r = -.08 p = .66	r = -.08 p = .67	r = .04 p = .83	r = .09 p = .65	r = -.11 p = .56
Right UNC	r = -.09 p = .08	r = -.01 p = .99	r = .10 p = .61	r = -.18 p = .35	r = .16 p = .38	r = -.15 p = .42	r = .01 p = .99	r = -.10 p = .61

DTI, diffusion tensor imaging; TOI, tract of interest; FA, fractional anisotropy; MD, mean diffusivity; AD, axial diffusivity; RD, radial diffusivity; PRSC, percentage reaction speed change; SLF, superior longitudinal fasciculus; ATR, anterior thalamic radiation; CST, corticospinal tract; IFOF, inferior fronto-occipital fasciculus; ILF, inferior longitudinal fasciculus; UNC, uncinate fasciculus. "*" indicates $p < 0.05$ and "*" indicates $p < 0.01$.

SLF-II and SLF-III are implicated in the maintenance of awareness and attention (Burzynska et al., 2011; Schmahmann and Pandya, 2006), which are directly relevant to wakefulness, attentive cognition, and vigilance. Damage to SLF-II and SLF-III has been linked to cognitive impairment due to disruption of the connections between the parietal cortex and the DLPFC and VLPFC (Karlsgodt et al., 2008). Our current finding is consistent with this existing knowledge and suggests that individual differences in the microstructure of the SLF-II and SLF-III subcomponents possibly contribute to the ability to sustain cognitive performance during extended wakefulness.

In the fiber bundle connecting fronto-parietal regions, higher FA and lower RD were associated with better cognitive resistance to SD. High levels of FA have been shown to occur in tightly bundled, structurally compact fibers (Pierpaoli and Basser, 1996; Pierpaoli et al., 1996). Lower RD is considered to reflect a higher degree of myelination (Beaulieu, 2002; Nair et al., 2005; Song et al., 2002). Myelination is one important factor in the regulation of axon conduction speed among fibers (Lang and Rosenbluth, 2003; Paus, 2010). Speed of signal transduction along the axon is a critical variable in information processing, both within cortical circuits and between distinct regions (Baker and Edgley, 2006; Sugihara et al., 1993). Therefore, a higher degree of myelination within the SLF may contribute to a faster signal transduction within the fronto-parietal network. This potential mechanism suggests that better cognitive resistance to SD is possibly associated with more efficient signal transduction between frontal and parietal cortices.

Finally, our findings also suggest that resistance to SD is mediated primarily through the left-hemisphere fronto-parietal attention network. In

our results, the activation of IPL and DLPFC that correlated with resistance was located in the left hemisphere. The reconstructed fronto-parietal connections, in which the DTI metrics are correlated with resistance, were also found in the left hemisphere. This finding was consistent with the existing studies that fronto-parietal activation associated with cognitive performance decline following SD was observed in the left hemisphere (Chee and Choo, 2004; Chee et al., 2006).

Our approach was only one of many possible ways to define cognitive vulnerability versus resistance to sleep deprivation. We chose to define degradation based on an average metric of mean global response slowing relative to baseline rather than on potentially more extreme change indices, such as the difference between maximal and minimum performance, because these latter approaches could have been more prone to capitalizing on chance fluctuations and temporary changes in performance that are more likely to emerge due to the instability of performance induced by sleep loss (Doran et al., 2001). Our goal was to define vulnerability in terms of stable degradation of performance relative to baseline. Thus, our speed-based metric was defined relative to the average baseline performance of the available sessions occurring prior to 11 pm, a common point where most normally sleeping individuals notice a rapid decline in alertness (Wesensten et al., 2005). Furthermore, we wanted our results to apply beyond the worst-case scenario defined by the low point of the circadian nadir, and therefore, included all time points through the morning, despite some improvement in performance due to the upswing of the circadian rhythm of alertness in the late morning. If anything, this potentially weakened our observed effects, but bolsters the generalizability of our findings beyond just the circadian nadir and worst-case scenarios.

Table 4
DTI metrics of fiber tracts connecting pairwise activation clusters in SWMT.

Paired seed regions	Mean \pm SD	Correlation with PRSC	Correlation with lapse	Correlation with activation in seed region	
Left DLPFC and left IPL MNP = 26				Left DLPFC	Left IPL
FA	.40 \pm 0.02	r = .41; p = .02*	r = -.25; p = .18	r = .30; p = .10	r = .08; p = .67
MD	.71 \pm 0.02	r = -.30; p = .11	r = .13; p = .50	r = -.31; p = .09	r = -.33; p = .08
AD	1.04 \pm 0.03	r = -.03; p = .88	r = -.04; p = .83	r = -.16; p = .40	r = -.30; p = .11
RD	.55 \pm 0.03	r = -.36; p = .05*	r = .18; p = .34	r = -.35; p = .06	r = .25; p = .19
Right VLPFC and right IPL MNP = 23				Right VLPFC	Right IPL
FA	.39 \pm 0.02	r = .04; p = .83	r = .08; p = .69	r = -.15; p = .43	r = -.33; p = .08
MD	.80 \pm 0.02	r = -.03; p = .88	r = -.09; p = .65	r = .26; p = .16	r = .35; p = .06
AD	1.15 \pm 0.02	r = -.01; p = .94	r = -.01; p = .97	r = .15; p = .42	r = .12; p = .54
RD	.62 \pm 0.03	r = -.02; p = .93	r = -.11; p = .56	r = .26; p = .17	r = .09; p = .64
Left VLPFC and left IPL MNP = 19				Left VLPFC	Left IPL
FA	.39 \pm 0.02	r = .24; p = .21	r = -.13; p = .50	r = .09; p = .62	r = .24; p = .21
MD	.81 \pm 0.03	r = -.15; p = .42	r = .11; p = .56	r = -.30; p = .11	r = -.22; p = .24
AD	1.18 \pm 0.05	r = .01; p = .98	r = .04; p = .84	r = -.26; p = .17	r = -.12; p = .53
RD	.63 \pm 0.03	r = -.24; p = .20	r = .15; p = .44	r = -.23; p = .22	r = -.26; p = .17
MFG and right IPL MNP = 5				MFG	Right IPL
FA	.42 \pm 0.02	r = .19; p = .32	r = -.17; p = .38	r = .03; p = .86	r = .05; p = .80
MD	.92 \pm 0.05	r = .01; p = .95	r = -.03; p = .89	r = -.27; p = .15	r = -.30; p = .11
AD	1.34 \pm 0.06	r = .07; p = .72	r = -.09; p = .64	r = -.28; p = .13	r = -.31; p = .10
RD	.71 \pm 0.05	r = -.02; p = .90	r = .01; p = .94	r = -.24; p = .21	r = -.27; p = .15
MFG and left IPL MNP = 4				MFG	Left IPL
FA	.39 \pm 0.02	r = .12; p = .54	r = .09; p = .64	r = .06; p = .76	r = -.01; p = .95
MD	.82 \pm 0.03	r = .22; p = .23	r = -.27; p = .15	r = -.10; p = .60	r = -.04; p = .84
AD	1.06 \pm 0.05	r = .20; p = .29	r = -.23; p = .23	r = -.13; p = .48	r = -.11; p = .57
RD	.69 \pm 0.03	r = .22; p = .25	r = -.26; p = .16	r = -.06; p = .75	r = .02; p = .90

DTI, diffusion tensor imaging; SWMT, Sternberg working memory task; PRSC, percentage reaction speed change; MNP, the maximum of probability values; FA, fractional anisotropy; MD, mean diffusivity; AD, axial diffusivity; RD, radial diffusivity; VLPFC, ventrolateral prefrontal cortex; DLPFC, dorsolateral prefrontal cortex; IPL, inferior parietal lobule; MFG, medial frontal gyrus. MD, AD and RD values were in $\text{mm}^2/\text{s} \times 10^{-3}$.

There are several limitations to the present study that should be considered. First, the voxel size of diffusion images ($1.75 \times 1.75 \times 3.5$ mm) is not isotropic in this study, which may affect the measurement of diffusion anisotropy (Oouchi et al., 2007). Second, we focused on the relationship between white matter microstructure and cognitive resistance to SD in this study and did not perform fMRI scanning after SD. Consequently, the fronto-parietal activation change following SD and its association with white matter was not investigated. Third, the working memory task performed in the current investigation was the Sternberg task. It is known that the activation elicited by WM is task-dependent (Lythe et al., 2012). There may exist other brain regions and neuronal tracts associated with resistance to SD that were not directly engaged by the SWMT. Thus, we also examined several other major fiber tracts using TOI-based measurement, but no other tract was found to be correlated with resistance to SD. Future research using alternate WM tasks would be helpful to investigate the specificity of this effect. Fourth, we did not analyze deactivation in this study. Deactivation refers to a reduction of BOLD signal during task performance relative to the baseline (Gusnard et al., 2001). A previous study found that reduced deactivation in the anterior medial frontal and posterior cingulate, which comprise major nodes of the default mode network, is correlated with slower individual performance in the WM task (Chee and Choo, 2004). In future work, we will also include analysis of deactivation to further explore the mechanisms of individual differences in resistance to SD. Another potential limitation of the present study is that we did not consider the role of gray matter volume in predicting resistance to SD. To our knowledge, there are no published neuroimaging studies examining the role of gray matter volume or cortical thickness as a predictor of the ability to resist sleep loss. To date, most neuroimaging studies predicting resistance to sleep loss have focused on functional brain activation or white matter integrity as measured by DTI, but have not included gray matter volume in their analyses. It is therefore not known how gray matter volume may

contribute to the ability to sustain wakefulness. In a previous study, however, we found that self-reported levels of general daytime sleepiness were negatively correlated with gray matter volume in a region of the left gyrus rectus and medial orbitofrontal cortex (Killgore et al., 2012). The observed association between gray matter volume and sleepiness raises the possibility that cortical volume in prefrontal regions may be related to the ability to resist sleep deprivation. This is clearly an area for further study. Finally, it could be argued that our use of square-root transformed lapses was unnecessary for statistical reasons and that the analysis could have been legitimately conducted on the raw lapse data as well (Williams et al., 2013). Accordingly, we ran our analyses both ways, finding essentially the same results. Since the effect of the transformation was inconsequential and transformed lapse data are commonly reported in the literature due to the strongly skewed distributions, we decided to present the transformed data in this manuscript.

Conclusion

This study employed a multimodal imaging approach to investigate the effect of white matter microstructure and functional cortical activation on the ability to resist the degrading effects of SD on psychomotor vigilance performance. In accordance with prior work, fronto-parietal activation at rested wakefulness during a WM task was predictive of reduced individual cognitive decline following SD. We provide novel information regarding the primary fiber bundle comprising the SLF, which connects frontal and parietal activated regions and contributes to this resistance capacity. Individuals with a higher level of microarchitecture in the SLF demonstrated better cognitive resistance to SD. Our findings reveal that the ability to sustain performance during sleep loss is not only associated with greater baseline rested activation in the fronto-parietal regions but also associated with the microstructural properties of their interconnecting axonal pathways.

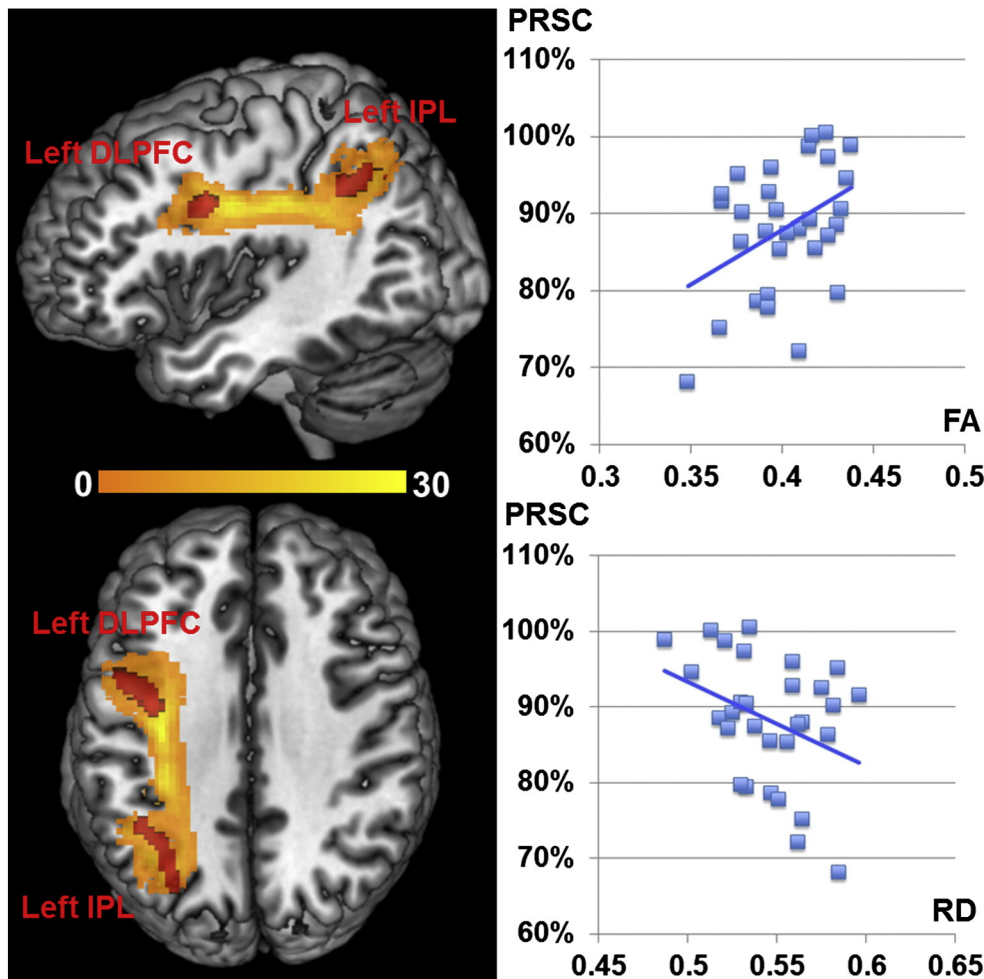


Fig. 5. Illustration demonstrating the population probability map of the left SLF, generated from probabilistic tractography of $N = 30$ participants. The heatmap shows the number of participants common to the reconstructed tract in each voxel. The coordinates are in MNI space. The seed regions for the tractography, left DLPFC and left IPL, were defined based on the fMRI results (Table 2). Scatterplots show the relationships between FA values of the SLF and PRSC ($r = .41$; $p = .02$); and between RD values of the left SLF and PRSC ($r = -.36$; $p = .05$). PRSC, percentage reaction speed change; SLF, superior longitudinal fasciculus; MNI, Montreal Neurological Institute; DLPFC, dorsolateral prefrontal cortex; IPL, inferior parietal lobule; FA, fractional anisotropy; RD, radial diffusivity.

Supplementary data to this article can be found online at <http://dx.doi.org/10.1016/j.neuroimage.2014.11.035>.

Funding

This research was supported by a DARPA Young Faculty Award to W.D.S.K. (D12AP00241).

Conflicts of interests

None declared.

References

- Baker, M.R., Edgley, S.A., 2006. Non-uniform olivocerebellar conduction time in the vermis of the rat cerebellum. *J. Physiol.* 570, 501–506.
- Basser, P.J., 1995. Inferring microstructural features and the physiological state of tissues from diffusion-weighted images. *NMR Biomed.* 8, 333–344.
- Basser, P.J., Mattiello, J., LeBihan, D., 1994. MR diffusion tensor spectroscopy and imaging. *Biophys. J.* 66, 259–267.
- Beaulieu, C., 2002. The basis of anisotropic water diffusion in the nervous system – a technical review. *NMR Biomed.* 15, 435–455.
- Behrens, T.E., Berg, H.J., Jbabdi, S., Rushworth, M.F., Woolrich, M.W., 2007. Probabilistic diffusion tractography with multiple fibre orientations: what can we gain? *NeuroImage* 34, 144–155.
- Budde, M.D., Kim, J.H., Liang, H.F., Schmidt, R.E., Russell, J.H., Cross, A.H., Song, S.K., 2007. Toward accurate diagnosis of white matter pathology using diffusion tensor imaging. *Magn. Reson. Med.* 57, 688–695.
- Burzynska, A.Z., Nagel, I.E., Preuschhof, C., Li, S.C., Lindenberger, U., Backman, L., Heekeren, H.R., 2011. Microstructure of frontoparietal connections predicts cortical reactivity and working memory performance. *Cereb. Cortex* 21, 2261–2271.
- Caldwell, J.A., Mu, Q., Smith, J.K., Mishory, A., Caldwell, J.L., Peters, G., Brown, D.L., George, M.S., 2005. Are individual differences in fatigue vulnerability related to baseline differences in cortical activation? *Behav. Neurosci.* 119, 694–707.
- Chee, M.W., Choo, W.C., 2004. Functional imaging of working memory after 24 hr of total sleep deprivation. *J. Neurosci.* 24, 4560–4567.
- Chee, M.W., Chuah, L.Y., Venkatraman, V., Chan, W.Y., Philip, P., Dinges, D.F., 2006. Functional imaging of working memory following normal sleep and after 24 and 35 h of sleep deprivation: Correlations of fronto-parietal activation with performance. *NeuroImage* 31, 419–428.
- Choo, W.C., Lee, W.W., Venkatraman, V., Sheu, F.S., Chee, M.W., 2005. Dissociation of cortical regions modulated by both working memory load and sleep deprivation and by sleep deprivation alone. *NeuroImage* 25, 579–587.
- Dinges, D.F., Powell, J.W., 1985. Microcomputer analyses of performance on a portable, simple, visual RT task during sustained operations. *Behav. Res. Methods Instrum. Comput.* 17, 652–655.
- Doran, S.M., Van Dongen, H.P., Dinges, D.F., 2001. Sustained attention performance during sleep deprivation: evidence of state instability. *Arch. Ital. Biol.* 139, 253–267.
- Gusnard, D.A., Akbudak, E., Shulman, G.L., Raichle, M.E., 2001. Medial prefrontal cortex and self-referential mental activity: relation to a default mode of brain function. *Proc. Natl. Acad. Sci. U. S. A.* 98, 4259–4264.
- Hagmann, P., Jonasson, L., Maeder, P., Thiran, J.P., Wedeen, V.J., Meuli, R., 2006. Understanding diffusion MR imaging techniques: from scalar diffusion-weighted imaging to diffusion tensor imaging and beyond. *Radiographics* 26 (Suppl. 1), S205–S223.
- Hua, K., Zhang, J., Wakana, S., Jiang, H., Li, X., Reich, D.S., Calabresi, P.A., Pekar, J.J., van Zijl, P.C., Mori, S., 2008. Tract probability maps in stereotaxic spaces: analyses of white matter anatomy and tract-specific quantification. *NeuroImage* 39, 336–347.

- Johansen-Berg, H., Della-Maggiore, V., Behrens, T.E., Smith, S.M., Paus, T., 2007. Integrity of white matter in the corpus callosum correlates with bimanual co-ordination skills. *NeuroImage* 36 (Suppl. 2), T16–T21.
- Karlsgodt, K.H., van Erp, T.G., Poldrack, R.A., Bearden, C.E., Nuechterlein, K.H., Cannon, T.D., 2008. Diffusion tensor imaging of the superior longitudinal fasciculus and working memory in recent-onset schizophrenia. *Biol. Psychiatry* 63, 512–518.
- Killgore, W.D.S., 2010. Effects of sleep deprivation on cognition. *Prog. Brain Res.* 185, 105–129.
- Killgore, W.D.S., 2011. Caffeine and other alerting agents. In: Thorpy, M.J., Billiard, M. (Eds.), *Sleepiness: Causes, Consequences and Treatment*. Cambridge University Press, New York, pp. 430–443.
- Killgore, W.D., Schwab, Z.J., Kipman, M., DelDonno, S.R., Weber, M., 2012. Voxel-based morphometric gray matter correlates of daytime sleepiness. *Neurosci. Lett.* 518, 10–13.
- Kim, D.S., Kim, M., 2005. Combining functional and diffusion tensor MRI. *Ann. N. Y. Acad. Sci.* 1064, 1–15.
- Lang, E.J., Rosenbluth, J., 2003. Role of myelination in the development of a uniform olivocerebellar conduction time. *J. Neurophysiol.* 89, 2259–2270.
- Loh, S., Lamond, N., Dorrian, J., Roach, G., Dawson, D., 2004. The validity of psychomotor vigilance tasks of less than 10-minute duration. *Behav. Res. Methods Instrum. Comput.* 36, 339–346.
- Lythe, K.E., Williams, S.C., Anderson, C., Libri, V., Mehta, M.A., 2012. Frontal and parietal activity after sleep deprivation is dependent on task difficulty and can be predicted by the fMRI response after normal sleep. *Behav. Brain Res.* 233, 62–70.
- Makris, N., Kennedy, D.N., McInerney, S., Sorensen, A.G., Wang, R., Caviness Jr., V.S., Pandya, D.N., 2005. Segmentation of subcomponents within the superior longitudinal fascicle in humans: a quantitative, in vivo, DT-MRI study. *Cereb. Cortex* 15, 854–869.
- Mayer, K.M., Vuong, Q.C., 2013. TBSS and probabilistic tractography reveal white matter connections for attention to object features. *Brain Struct. Funct.* 219, 2159–2171.
- Mu, Q., Mishory, A., Johnson, K.A., Nahas, Z., Kozel, F.A., Yamanaka, K., Bohning, D.E., George, M.S., 2005. Decreased brain activation during a working memory task at rested baseline is associated with vulnerability to sleep deprivation. *Sleep* 28, 433–446.
- Nair, G., Tanahashi, Y., Low, H.P., Billings-Gagliardi, S., Schwartz, W.J., Duong, T.Q., 2005. Myelination and long diffusion times alter diffusion-tensor-imaging contrast in myelin-deficient shiverer mice. *NeuroImage* 28, 165–174.
- Oouchi, H., Yamada, K., Sakai, K., Kizu, O., Kubota, T., Ito, H., Nishimura, T., 2007. Diffusion anisotropy measurement of brain white matter is affected by voxel size: underestimation occurs in areas with crossing fibers. *AJNR Am. J. Neuroradiol.* 28, 1102–1106.
- Paus, T., 2010. Growth of white matter in the adolescent brain: myelin or axon? *Brain Cogn.* 72, 26–35.
- Pierpaoli, C., Bassler, P.J., 1996. Toward a quantitative assessment of diffusion anisotropy. *Magn. Reson. Med.* 36, 893–906.
- Pierpaoli, C., Jezzard, P., Bassler, P.J., Barnett, A., Di Chiro, G., 1996. Diffusion tensor MR imaging of the human brain. *Radiology* 201, 637–648.
- Rocklage, M., Williams, V., Pacheco, J., Schnyer, D.M., 2009. White matter differences predict cognitive vulnerability to sleep deprivation. *Sleep* 32, 1100–1103.
- Rupp, T.L., Wesensten, N.J., Balkin, T.J., 2012. Trait-like vulnerability to total and partial sleep loss. *Sleep* 35, 1163–1172.
- Schmahmann, J.D., Pandya, D.N., 2006. *Fiber Pathways of the Brain*. Oxford University Press, New York.
- Schmahmann, J.D., Pandya, D.N., Wang, R., Dai, G., D'Arceuil, H.E., de Crespigny, A.J., Wedeen, V.J., 2007. Association fibre pathways of the brain: parallel observations from diffusion spectrum imaging and autoradiography. *Brain* 130, 630–653.
- Schmithorst, V.J., Yuan, W., 2010. White matter development during adolescence as shown by diffusion MRI. *Brain Cogn.* 72, 16–25.
- Sheehan, D.V., Lecrubier, Y., Sheehan, K.H., Amorim, P., Janavs, J., Weiller, E., Hergueta, T., Baker, R., Dunbar, G.C., 1998. The Mini-International Neuropsychiatric Interview (M.I.N.I.): the development and validation of a structured diagnostic psychiatric interview for DSM-IV and ICD-10. *J. Clin. Psychiatry* 59 (Suppl. 20), 22–33 (quiz 34–57).
- Smith, S.M., 2002. Fast robust automated brain extraction. *Hum. Brain Mapp.* 17, 143–155.
- Smith, S.M., Jenkinson, M., Woolrich, M.W., Beckmann, C.F., Behrens, T.E., Johansen-Berg, H., Bannister, P.R., De Luca, M., Drobnjak, I., Flitney, D.E., Niazy, R.K., Saunders, J., Vickers, J., Zhang, Y., De Stefano, N., Brady, J.M., Matthews, P.M., 2004. Advances in functional and structural MR image analysis and implementation as FSL. *NeuroImage* 23 (Suppl. 1), S208–S219.
- Song, S.K., Sun, S.W., Ramsbottom, M.J., Chang, C., Russell, J., Cross, A.H., 2002. Demyelination revealed through MRI as increased radial (but unchanged axial) diffusion of water. *NeuroImage* 17, 1429–1436.
- Song, S.K., Sun, S.W., Ju, W.K., Lin, S.J., Cross, A.H., Neufeld, A.H., 2003. Diffusion tensor imaging detects and differentiates axon and myelin degeneration in mouse optic nerve after retinal ischemia. *NeuroImage* 20, 1714–1722.
- Stern, Y., 2002. What is cognitive reserve? Theory and research application of the reserve concept. *J. Int. Neuropsychol. Soc.* 8, 448–460.
- Sugihara, I., Lang, E.J., Llinas, R., 1993. Uniform olivocerebellar conduction time underlies Purkinje cell complex spike synchronicity in the rat cerebellum. *J. Physiol.* 470, 243–271.
- Van Dongen, H.P., 2005. Brain activation patterns and individual differences in working memory impairment during sleep deprivation. *Sleep* 28, 386–388.
- Van Dongen, H.P., Baynard, M.D., Maislin, G., Dinges, D.F., 2004. Systematic interindividual differences in neurobehavioral impairment from sleep loss: evidence of trait-like differential vulnerability. *Sleep* 27, 423–433.
- Wesensten, N.J., Killgore, W.D.S., Balkin, T.J., 2005. Performance and alertness effects of caffeine, dextroamphetamine, and modafinil during sleep deprivation. *J. Sleep Res.* 14, 255–266.
- Williams, M.N., Grajales, C.A.G., Kurkiewicz, D., 2013. Assumptions of multiple regression: correcting two misconceptions. *Pract. Assess. Res. Eval.* 18, 1–14.